

1 **Sensitivity of flood loss estimates to building representation and flow depth**  
2 **attribution methods in micro-scale flood modelling**

3 María Bermúdez<sup>1\*</sup>, Andreas Paul Zischg<sup>2</sup>

4 <sup>1</sup> Water and Environmental Engineering Group, University of A Coruña, Spain. Email:  
5 mbermudez@udc.es. Phone: +34 981167000, Ext. 1427. ORCID: 0000-0003-3189-  
6 4791

7 <sup>2</sup> Institute of Geography, Oeschger Centre for Climate Change Research, Mobiliar Lab  
8 for Natural Risks, University of Bern, Bern, CH-3012, Switzerland. ORCID: 0000-  
9 0002-4749-7670

10 \* corresponding author

11  
12 **Abstract**

13 Thanks to modelling advances and the increase of computational resources in recent years, it is now  
14 feasible to perform 2-D urban flood simulations at very high spatial resolutions and to conduct flood  
15 risk assessments at the scale of single buildings. In this study, we explore the sensitivity of flood loss  
16 estimates obtained in such micro-scale analyses to the spatial representation of the buildings in the 2D  
17 flood inundation model and to the hazard attribution methods in the flood loss model. The results show  
18 that building representation has a limited effect on the exposure values (i.e., the number of elements  
19 at risk), but can have a significant impact on the hazard values attributed to the buildings. On the other  
20 hand, the two methods for hazard attribution tested in this work result in remarkably different flood  
21 loss estimates. The sensitivity of the predicted flood losses to the attribution method is comparable to  
22 the one associated with the vulnerability curve. The findings highlight the need for incorporating these  
23 sources of uncertainty into micro-scale flood risk prediction methodologies.

24  
25 **Keywords:** inundation modelling, micro-scale, building representation, flood loss estimation  
26  
27  
28

## 29 **1. Introduction**

30 Flood inundation numerical models are a well-established approach for conducting flood risk analysis.  
31 Although one-dimensional hydrodynamic models are still in widespread use for many applications,  
32 the use of two-dimensional models is required in built-up areas to reproduce the complex,  
33 multidirectional flow paths generated by urban features (Apel et al. 2009). Thanks to modelling  
34 advances and the increase of computational resources in recent years, it is now feasible to perform 2-  
35 D urban flood simulations at resolutions as low as 10 cm (Ozdemir et al. 2013; de Almeida et al. 2016).  
36 Together with the increase of data availability, this has opened up the possibility of conducting flood  
37 risk analysis and assessing damages at the scale of the single building (micro-scale), without the need  
38 for spatial aggregation of elements at risk (Staffler et al. 2008; Merz et al. 2010; Zischg et al. 2013,  
39 2018, Fuchs et al. 2015, 2017; Röthlisberger et al. 2017). In micro-scale risk analyses, flood hazard is  
40 estimated by means of spatially detailed models solving the 2D shallow water equations. In addition,  
41 fine-resolution geospatial datasets are exploited to characterize the reconstruction value and the  
42 vulnerability of each building. Such a detailed analysis is relevant to reliably assess the effectiveness  
43 of flood protection measures for reducing flood risk in individual areas (Ernst et al. 2010). It can be  
44 used to objectively evaluate the economic cost-effectiveness of individual precautionary measures on  
45 buildings (i.e., retrofitting methods) (Arrighi et al. 2013), or be part of decision support systems to  
46 evaluate flood risk (Qi and Altinakar 2011).

47 The adoption of a micro-scale flood modelling approach allows the representation of small-scale  
48 structural elements and small topographic variations explicitly in the hydrodynamic model, instead of  
49 parameterizing their effects via subgrid scale models or artificial roughness (Abdullah et al. 2012;  
50 Abily et al. 2016). The value of roughness coefficient in such a 2D hydrodynamic model is thus set to  
51 represent only small scale roughness, its calibration being less important than for low spatial resolution  
52 models (Horritt and Bates 2002). This is relevant because of the lack of sufficient data for model  
53 calibration and validation in many locations. However, sensitivity to other model features, such as the  
54 mesh setup in relation to the building pattern and the building representation, may have a significant  
55 impact on the hydrodynamic results and, in turn, on the flood-loss results. A few studies deal with  
56 these effects in urban areas (Fewtrell et al. 2008, 2011; Sampson et al. 2012; Schubert and Sanders  
57 2012). However, these aspects have received far less attention for rural and peri-urban situations and  
58 have been generally explored in isolation from evaluation of uncertainties in loss estimation  
59 approaches.

60 Several methods have been proposed in recent years to represent buildings in shallow water models.  
61 A first group of methods parameterizes the effects of buildings on flooding by means of porosity

62 parameters (Cea and Vázquez-Cendón 2009; Schubert and Sanders 2012; Guinot 2012) or by building  
63 coverage and conveyance reduction factors (Chen et al. 2012a, b). This allows the simulation of urban  
64 flood flows with a relatively coarse mesh and hence a fast execution time. However, these methods  
65 are not suitable for micro-scale flood modelling, which aims at capturing the localized variability of  
66 flood depth and velocity around buildings. In this case, a so-called “resolved approach”, which  
67 explicitly considers the exact building geometries is needed (Schubert and Sanders 2012). The  
68 building-block method (BB) and the building-hole (BH) method are among the most used methods of  
69 this type. In the BB method, a digital surface model that incorporates the heights of the rooftops is  
70 used to produce a local elevation rise of the grid cells within building footprints. In the BH method,  
71 the area within the building footprints is excluded from the model domain, and closed boundary  
72 conditions are enforced at building walls. As noted by Bellos and Tsakiris (2015), reservations have  
73 been expressed for the BB and BH methods, related to the fact that they do not simulate flood flow  
74 inside the building and therefore any possible storage effects of the buildings are not taken into  
75 account. However, alternative methods such as the representation of the exterior walls of each building  
76 with an inlet on the front wall (Bellos and Tsakiris 2015), so that water can slip into the house, are  
77 seldom used in practical applications.

78 A key component of any flood risk analysis is the vulnerability assessment (Fuchs et al. 2012;  
79 Papathoma-Köhle et al. 2017) which is frequently focused only on direct flood loss. Depth-damage  
80 functions, which denote the flood damage that would occur at specific water depths per asset or per  
81 land-use class, are typically applied for this purpose. Other factors such as flow velocity are presumed  
82 to influence flood damage, but their general consideration in monetary loss modelling is not  
83 recommended (Kreibich et al. 2009). From a practitioner’s perspective, the application of depth-  
84 damage functions is therefore the standard approach to assessing urban flood loss. The development  
85 of site-specific depth-damage functions is not feasible at many locations, and the use of models  
86 developed elsewhere is common practice in literature (Apel et al. 2006; Notaro et al. 2014). In fact,  
87 libraries of depth-damage curves are available for different regions (Davis and Skaggs 1992; Green  
88 2003). In addition to the inherent uncertainty in the depth-damage curves, their extrapolation to regions  
89 where building characteristics are not necessarily the same raises concerns regarding their local  
90 representativeness (Cammerer et al. 2013; McGrath et al. 2015). Various studies have already  
91 acknowledged the uncertainty and limitations associated with the use of depth-damage curves in flood  
92 damage estimation (de Moel and Aerts 2011; Sampson et al. 2014). Freni et al. (2010) suggest that the  
93 use of highly detailed 2D hydraulic models in flood risk assessments might not be justified if depth-  
94 damage curves are used to assess damages, given the significant uncertainties of the later.

95 In addition to the selection of a suitable depth damage curve, other modelling choices need to be made  
96 in flood risk assessments. It is necessary to define how the number of exposed buildings will be counted  
97 and how the inundation characteristics will be assigned to each exposed building. Exposure  
98 information is essentially provided through the overlapping of the building footprint and the hazard  
99 maps. The high spatial resolution of the hazard results in micro-scale flood assessments allows  
100 however for different exposure evaluation, i.e. building counting, methods. A building can be assumed  
101 to be affected by the inundation if water depths computed within its footprint are above a certain wet-  
102 dry threshold. More sophisticated methods consider a buffer distance between the building edges and  
103 the flooded areas or calculate the proportion of the external perimeter of a property that is wet in the  
104 case of partially flooded buildings (Environment Agency 2014). On the other hand, the assignment of  
105 flow characteristics (water depths in the general case) to each building may be performed in different  
106 ways. This is referred to as flow depth attribution method in this paper. In the micro-scale flood risk  
107 analysis performed by Ernst et al. (2010), the water depth in the building is obtained either by  
108 averaging the water depth in the neighboring cells or by linearly interpolating the ground level and the  
109 free surface elevation inside the asset. The aforementioned differences in attribution methods can  
110 potentially result in very different flood damage estimates. Yet, to the best of our knowledge, there are  
111 no studies available that have quantified its impact on the flood loss predictions.

112 Hence, the main research question for this paper is how flood loss estimates are influenced by the  
113 building representation and the flow depth attribution methods. To answer this question, we conduct a  
114 micro-scale flood loss assessment in a low density residential case study that is typical for rural and  
115 peri-urban hilly landscapes in Europe. The modelling framework comprises a flood inundation model  
116 and a flood loss model, which provide hazard and impact estimates for a given flood event at a high  
117 spatial resolution. We analyze the sensitivity of the predicted flood loss to the building representation  
118 in the flood inundation model and to the vulnerability function and attribution method in the flood loss  
119 model. The benefits and limitations of the different methods are evaluated, and the applicability for  
120 real-world case studies is discussed. The main aim of this work is to contribute to the development of  
121 consistent frameworks for micro-scale flood risk assessments, with a balanced accuracy and spatial  
122 detail of the different steps of the modelling process.

123

## 124 **2. Methods**

125 The model experiment was set up on the basis of a flood inundation model and a flood loss model  
126 (Figure 1). Both sub-modules were altered in the experiment. While we kept the upstream boundary

127 condition of the flood inundation model constant, i.e. the inflow hydrograph, we varied the  
128 computational mesh with different representations of the buildings. In the flood loss module, the  
129 building dataset was kept constant while we varied the flow depth attribution methods and the  
130 vulnerability functions. The methodology is described in more detail below.

### 131 2.1. Study area

132 We set up the model experiment in the case study of Steffisburg, a community in the Canton of Bern  
133 in Switzerland. The study area covers an area of 4.8 km<sup>2</sup> and is located on the alluvial fan of the Zulg  
134 river (Figure 2). The fan has an average slope of 1.3 %. The Zulg river has a catchment area of 90  
135 km<sup>2</sup>. The main village of Steffisburg is located along the Zulg river sprawling towards south and the  
136 city of Thun. It has 15'700 inhabitants and 1682 buildings. The density of buildings is low in  
137 comparison to urban areas (~350 buildings per km<sup>2</sup>) but not as low as in rural areas. The average  
138 distance between three neighboring buildings is 14.4 m with a standard deviation of 12.6 m. In  
139 comparison, Schubert and Sanders (2012) computed an average gap between buildings in an urban  
140 environment of 3.8 m. Hence, the village can be classified as a typical peri-urban settlement. The  
141 majority of the buildings are of residential and combined residential/commercial use. In the south and  
142 the north of the study area, two clusters of industrial/commercial buildings are located.

### 143 2.2. Flood inundation model

144 A flood inundation model of the area was set up using the software Iber (Bladé et al. 2014). The model  
145 solves the 2D depth-averaged shallow water equations by means of a finite volume method. It  
146 computes the water depth and the two horizontal components of the depth-averaged velocity, the  
147 former constituting the basis for the flood hazard assessment in this work. The model Iber has been  
148 successfully applied in a wide range of flood modelling studies (Bodoque et al. 2016; González-  
149 Aguirre et al. 2016; Álvarez et al. 2017; Bonasia et al. 2017), including detailed flood assessments in  
150 urban areas, in which the flow depth field was evaluated at the scale of the streets and buildings  
151 (Garrote et al. 2016; Bermúdez et al. 2017). For a detailed description of the model and additional  
152 validation examples we refer to Bladé et al. (2014) and Cea et al. (2016), and the references therein.  
153 The model is run in an uncalibrated mode using typical physical values for the Manning roughness  
154 coefficient, as proposed by Zischg et al. (2018). This is justified due to the low sensitivity of the model  
155 to the friction parameter and the absence of documented flood events that could be used for validation.

156 We set up the flood inundation model at the micro-scale, which implies that exposure and hazard must  
157 be assessed at the scale of individual elements at risk such as buildings or infrastructures. The flood  
158 model must therefore represent flows at this targeted spatial scale. The domain was discretized

159 accordingly by an unstructured computational mesh at a very high spatial resolution, with mesh sizes  
160 of 2.5 m in the built up areas and the river channel, and between 5 and 10 m in the non-urbanized areas.  
161 Element size is thus smaller than the critical length scales determined by building dimensions and  
162 building separation distances (Fewtrell et al. 2008). The total number of elements in the mesh is  
163 approximately 1'000'000, the exact number is depending on the mesh setup explained below. We used  
164 a 0.5 m-resolution digital elevation model (DEM) derived from LiDAR and a building footprint map  
165 to define the model geometry. Two different DEMs were used in this study: a “bare-earth” digital  
166 terrain model (DTM) and a digital surface model (DSM) which incorporates the elevation of the  
167 buildings (i.e., the heights of the rooftops). Four different mesh configurations were considered (Figure  
168 3 and 4), which differ on the building representation, as follows:

- 169 - Mesh A: The building hole method BH is used to represent the buildings. Buildings are thus  
170 void areas in the mesh and buildings' walls fit exactly with numerical mesh edges.
- 171 - Mesh B: Buildings are not represented in the model. For this purpose, the area covered by the  
172 buildings is not excluded from the calculation domain and the topography is defined from the  
173 DTM. The building footprint is still used to generate the mesh, so the mesh nodes located in  
174 the building walls stay at the same location as in mesh A.
- 175 - Mesh C: The building block method BB is used to represent the buildings. This means that the  
176 buildings are not excluded from the calculation domain, and they appear as blocks with the  
177 height of the roofs in the mesh. The building footprint is used to generate the mesh, so building  
178 walls are aligned with internal element edges in the mesh (Figure 4b). This allows a precise  
179 representation of the contours of the buildings in the mesh, as shown in Figure 3c.
- 180 - Mesh D: The building block method BB is used to represent the buildings, as in mesh C.  
181 However, the building footprint is not used to create the mesh, so mesh nodes are not forced to  
182 lie along the building footprint (Figure 4c). As a consequence, the mesh cannot fit exactly the  
183 walls of the buildings, no matter how fine the resolution of the mesh is. Building walls are thus  
184 subject to an effect similar to the ‘staircase effect’ that appears at curved and slanted interface  
185 boundaries on regular Cartesian grids (Kumar et al. 2009), as can be seen in Figure 3d.

186

### 187 2.3. Values at risk

188 In this study, we focus on losses to buildings. Damages on house content, infrastructure or indirect  
189 losses are not considered. Hence, the dataset of the values at risk consists of a spatial dataset  
190 representing the buildings and their characteristics. The building is spatially represented by its footprint  
191 polygon. This basic dataset was extracted from the terrain model of the Federal Office for Topography

192 (swisstopo). Adjacent polygons were merged to one polygon. We attributed the data of the residential  
193 register to the building footprints. These data were provided by the Federal Office for Statistics. This  
194 results in the number of residents per building. With this dataset, it was possible to classify all buildings  
195 with residential purpose. In a further step, we attributed the land use categories of the communal land  
196 use plans to each building. This leads to a distinction between buildings with residential, commercial,  
197 industrial and public purpose. Moreover, we attributed the volume of the building by computing the  
198 average difference between DSM and DTM and multiplying it with the footprint area. The  
199 reconstruction value of each building was successively computed on the basis of the volume and a  
200 typical price per volume differentiated by building category. The approach followed the methods  
201 presented in Fuchs et al. (2015), Fuchs et al. (2017), and Röthlisberger et al. (2017).

#### 202 2.4. Flood-loss model

203 The flood loss model combines the outcomes of the inundation model with the dataset of the values at  
204 risk. To allow the assessment of the uncertainties in the methods for representing the buildings in the  
205 mesh and in the methods for attributing flow depths to the buildings, the flood loss model has to be  
206 designed in a flexible way. The spatial representation of the buildings by their footprints is held  
207 constant in all methods for pre-processing the mesh. However, depending on the representation of the  
208 buildings in the mesh, the flow depth attribution method changes. Thus, the flood loss model allows  
209 to consider different setups. In all setups, a building is counted as affected by the flood process if (a)  
210 a mesh node within the building footprint or (b) a mesh node at the border of the building footprint has  
211 a flow depth  $> 0$ . In addition, the model allows the consideration of a building as affected if (c) a mesh  
212 node within a user-defined buffer distance is modelled as wet.

213 To account for the different building representation methods in one flood loss model, we set up the  
214 procedure described in the following steps. In a first step, the computational mesh of the IBER flood  
215 model is read in and a point dataset of nodes is created. Second, the nodes point dataset is intersected  
216 with the building footprint dataset and a topology table is created. Herein, two situations can be  
217 handled. The intersection between both datasets results in a new point dataset. This dataset contains  
218 all buildings that have nodes of the computational mesh located within its footprint polygon. All other  
219 buildings not having any nodes located within their footprints are considered in a further step. For  
220 these buildings, a near table is computed by considering a maximum buffer distance and a maximal  
221 number of nodes to consider in the neighborhood analysis. This results in a table listing the mesh nodes  
222 that are relevant for attributing the flow depths to the building. The buffer distance and the maximum  
223 number of points to be considered in the analysis can be defined by the user. In our study, we defined  
224 a search radius of 0.5 m and a maximum number of 100 nodes to consider in the neighborhood analysis.

225 Third, the simulation outputs of the IBER model, i.e. the flow depths per mesh node and time step are  
226 read into an array.

227 For each building it is iteratively searched in the topology tables if the building intersects directly or  
228 indirectly (neighborhood) with the mesh nodes. If the intersection between building and mesh nodes  
229 is a direct overlay, the flow depth is directly attributed to the building from the flow depths located  
230 within the building footprint. This can be done either by computing the average (MEAN) or the  
231 maximum flow depth of all nodes (MAX). If the building has no mesh nodes within its footprint, the  
232 flow depth is attributed from the neighboring mesh nodes. Herein, also the average or the maximum  
233 could be defined depending on the research question. However, in the case of the “MEAN” attribution  
234 method, the average is computed by inversely weighting the distance between the building and the  
235 mesh nodes. The flow depth attribution is done for each time step of the flood inundation simulation.  
236 Consequently, a flow depth hydrograph is extracted for each building. In a subsequent step, the  
237 maximum flow depth over all time steps for each building is used to compute the degree of loss by  
238 means of the vulnerability function.

239 In this study, we used the vulnerability functions of Totschnig et al. (2011), Papathoma-Köhle et al.  
240 (2015), Hydrotec (2001), as cited in Merz and Thielen (2009), Jonkman et al. (2008) and Dutta et al.  
241 (2003). We used different vulnerability functions because, on the one hand, we aim at assessing the  
242 uncertainties in this part of the flood loss model and, on the other hand, we do not have loss data to  
243 validate the loss function or to choose the function with the highest fit. However, each of the selected  
244 vulnerability functions allows us to delineate a degree of loss for each building depending on the  
245 magnitude of the flood, i.e. the flow depth at the building scale in our case. The degree of loss *dol*  
246 resulting from the vulnerability function and the flow depth is used to compute the loss of the building.  
247 This is done by multiplying the *dol* with the reconstruction value of each building. Finally, all losses  
248 computed at single building level are summed up at the level of the study area.

249 With these specifications, the flood loss module is able to consider all four approaches for representing  
250 the buildings in the loss modelling. In mesh A, only the mesh nodes within a distance of 0.5 m from  
251 the outline of the building footprint are considered in the flow depth attribution. In meshes B, C, and  
252 D, the mesh nodes within the building footprint or within a distance of 0.5 m from the outline are  
253 considered.

254

255

256 **3. Results and discussion**

257 The application of the flood loss model on the outcomes of four different flood inundation models,  
 258 combined with two flow depth attribution methods and five vulnerability functions resulted in forty  
 259 simulation results. The number of affected buildings ranges from 572 to 618, and the number of  
 260 exposed residents ranges from 3'373 to 3'502. The results of the exposure analyses are shown in table  
 261 1. Mesh setup D shows the lowest numbers of exposed buildings and residents, while mesh A shows  
 262 the highest. Although the variability in the exposure is below 8 %, this demonstrates that the procedure  
 263 is sensitive to the mesh setup and the approach of representing the buildings in the mesh.

264 Differences in flood extent between mesh A, C and D, which include different representations of the  
 265 buildings, are below 0.3%. On the other hand, mesh B shows an increase of the flooded area of around  
 266 10% with respect to the other mesh configurations. However, given that buildings are not represented  
 267 in mesh B, the internal area of affected buildings is counted as flooded area.

268

269 **Table 1.** Flood extent, number of exposed residents and number of affected buildings with the different  
 270 mesh configurations.

Mesh	Flood extent (m <sup>2</sup> )	# affected buildings	# exposed residents
A	1'107'339	618	3'502
B	1'242'711	592	3'447
C	1'107'045	589	3'391
D	1'110'062	572	3'373

271

272 In contrast to the flood exposure, the flow depths at single building vary markedly with the mesh set  
 273 up and the flow depth attribution method. Figure 5 shows a comparison between the mesh setups and  
 274 the flow depth attribution method. Obviously, the “MAX” flow depth attribution method results in  
 275 higher flow depths at building scale than the “MEAN” method. The differences are particularly high  
 276 for mesh C and mesh D, given that the dry nodes within the building footprint (nodes with the height  
 277 of the rooftops) are used in the calculation of the mean depth of the building. In these cases, the  
 278 “MEAN” method underestimates flow depths. In an additional calculation, we removed the nodes  
 279 within the buildings and counted only the nodes at the outline of the building footprint in mesh B and  
 280 C, or the neighboring mesh nodes in mesh D. If the nodes within the building are excluded from the  
 281 flood loss calculation, the flow depths are higher and more similar to the ones computed with mesh A  
 282 (see table 2). In the case of mesh B, the difference with the original mean depth value is very small,  
 283 given that the nodes within the footprint are assigned the height of the ground and can thus be flooded.

284 This leads to the conclusion that in averaging the flow depths (“MEAN” attribution method), the nodes  
 285 within the building footprints should be excluded if their z-coordinates represent the building heights  
 286 (BB method) and consequently do not exhibit relevant flow depths.

287 On average over all buildings, the flow depths attributed to the buildings by the “MAX” attribution  
 288 method are systematically and markedly higher than the ones computed with the “MEAN” method. It  
 289 should be noted that differences are also very relevant for mesh A, which has no nodes within the  
 290 building footprints, and for mesh B, in which the nodes of the building footprint are assigned the height  
 291 of the ground and can thus be flooded. In this relatively steep study area, the range of z-coordinates at  
 292 the outlines of the building footprints (i.e., the difference between the minimum and maximum altitude  
 293 of the building footprint) is 0.78 m on average. Large buildings have a length of up to 80 m, which  
 294 results in an altitude difference of up to 8.8 m. This significant variation in z-coordinates across the  
 295 footprints results in variable flow depths within a single building. A significant portion of all buildings  
 296 is only partially wet. It is concluded from the above that, as the flow depth is relevant for the  
 297 computation of the degree of loss, the flood loss computation is highly sensitive to the flow attribution  
 298 method.

299 **Table 2.** Average depth (m) attributed to buildings.

Mesh	Flow depth [m] “MAX” attribution method	Flow depth [m] “MEAN” attribution method	Flow depth [m] “MEAN” attribution method (nodes within buildings excluded)
Mesh A	0.623	0.248	not applicable
Mesh B	0.624	0.190	0.192
Mesh C	0.667	0.088	0.242
Mesh D	0.655	0.046	0.263

300

301 When comparing the flow depths at building scale of the different mesh setups, the relevance of the  
 302 flow depth attribution method becomes obvious again (see Figure 6). However, the “MAX” attribution  
 303 method has a relatively low sensitivity to the mesh setup. The flow depths assigned to buildings are  
 304 very similar for all four mesh setups. In contrast, the “MEAN” attribution method implies a higher  
 305 sensitivity as mesh C and D result in significantly lower depths in buildings than mesh A and B. The  
 306 averaged flow depths (“MEAN”) differ markedly between the mesh setup, whereas the maximum flow  
 307 depths (“MAX”) do not vary significantly. Hence, the latter flow depth assignment method produces  
 308 robust estimations. It should be noted, however, that this robustness does not imply that the accuracy

309 of the method is necessarily superior. If flow depths vary significantly across a single building, the  
 310 depths obtained with the “MAX” attribution method might not be representative for damage  
 311 assessment, and produce an overestimation of losses.

312 The generally higher flow depths computed with the “MAX” assignment method result consequently  
 313 in higher losses. Table 3 shows the computed flood losses on buildings summed up for the study area.  
 314 The overall losses range from 800'000 CHF to 284 million CHF. This is a remarkable uncertainty  
 315 range and thus it underlines the importance of this sensitivity analysis. The flood loss computation is  
 316 markedly sensitive to both the vulnerability function and the flow depth attribution method. While the  
 317 first observation is in line with other studies (Apel et al. 2008, 2009; de Moel and Aerts 2011), the  
 318 second observation adds new insights in the discussion of uncertainties in flood loss modelling.  
 319 Depending on the flow depth attribution method, the total loss differs by two orders of magnitude.  
 320 This can be explained by the differences in the flow depths at the single buildings. Especially, the  
 321 consideration of mesh nodes within building footprint has to be avoided in averaging flow depths if  
 322 these mesh nodes do not represent the z-coordinates of the ground floor but those of the roof top.

323 However, if only one vulnerability function and one flow depth attribution method is considered  
 324 distinctly, but the mesh set up is varied, the losses result as relatively robust. While mesh A is the most  
 325 conservative in terms of number of exposed buildings and residents, it is not the most conservative in  
 326 total losses. Mesh C with the “MAX” attribution method results in the highest losses.

327 **Table 3.** Total flood losses in million Swiss Francs (CHF).

Mesh	Hazard attribution	Vulnerability function					Mean ± standard deviation
		Totschnig et al. (2011)	Papathoma-Köhle et al. (2015)	Hydrotec (2001)	Jonkman et al. (2008)	Dutta et al. (2003)	
A	MAX	264.9	248.3	241.0	73.0	237.8	213.0±78.9
	MEAN	33.2	41.9	123.5	14.0	100.1	62.5±46.8
B	MAX	265.5	247.2	235.4	70.5	233.6	210.4±79.3
	MEAN	21.9	28.6	103.5	10.6	81.5	49.2±40.8
C	MAX	284.0	263.8	243.9	76.8	243.7	222.4±83.1
	MEAN	2.9	5.0	60.5	4.9	42.3	23.1±26.6
D	MAX	248.0	238.0	236.5	80.3	228.1	206.2±70.7
	MEAN	0.8	1.6	38.5	2.9	26.9	14.2±17.4

328

329 From the viewpoint of the vulnerability functions, the one described by Jonkman et al. (2008) results  
 330 in the lowest losses. This function was elaborated on data in the Netherlands. Still, the presented case  
 331 study in an Alpine environment might differ markedly from a lowland situation in terms of process

332 characteristics. The functions of Totschnig et al. (2011) and Papathoma-Köhle (2015) consider  
333 torrential processes and sediment transport and might be more adequate for this case study.  
334 Nevertheless, as Cammerer et al. (2013) and Amadio et al. (2016) discussed, the transferability of  
335 vulnerability functions may be questioned in any case. However, the choice of the vulnerability  
336 function and a validation was out of scope of this study and the focus was laid on the comparison of  
337 different uncertainty sources.

338 From the view point of the real-world applicability, the four building representation methods applied  
339 in this work have distinct advantages and disadvantages, and the choice of method will depend on the  
340 available data and the particular application. All four methods result in computationally demanding  
341 simulations, given the grid size required to capture the complex flow between buildings. For  
342 applications that require multiple simulations or fast results, the development of computationally more  
343 efficient surrogates of these models might become necessary (Bermúdez et al. 2018). Model setup  
344 complexity does vary significantly between the methods, and is thus likely to be a more relevant  
345 criterion for choosing an approach. If a suitable DSM is available, the approach corresponding to mesh  
346 D (i.e., the BB method without building geometry data) is the easiest to implement, given that building  
347 footprints are not used to constrain the mesh. However, in order to capture precisely the contours of  
348 the buildings, a very fine grid is needed. On the other hand, methods which make use of building  
349 footprints to produce sharp elevation changes at building interfaces (mesh A and C in this work) are  
350 more demanding from a pre-processing perspective. However, they could potentially allow for a  
351 certain mesh size optimization, up to the critical grid sizes defined by building dimensions and  
352 separation distances, as noted by Fewtrell et al. (2008). This aspect is beyond the scope of this work,  
353 and no coarsening was applied in this study to ensure consistency between the four mesh  
354 configurations. The number of mesh elements can be further reduced if the buildings are represented  
355 as holes in the mesh (as in mesh A). However, this may be a disadvantage for certain applications,  
356 such as the computation of rainfall-runoff transformation from direct precipitation over the model  
357 domain. If the mesh excludes the areas covered by the buildings, the rainfall fields need to be modified  
358 to account for the artificial loss of area.

359

#### 360 **4. Conclusions**

361 The presented model experiment allowed to assess and compare two uncertainty sources in flood loss  
362 modelling at the micro-scale. We analyzed the sensitivity of a typical flood loss modelling setup to the

363 method for representing the buildings in the computational mesh of 2D flood models and to the method  
364 for assigning flow depths from the simulation outcomes to the single buildings.

365 The model experiment leads to the following main conclusions.

366 1) At the micro-scale, the topology between a building footprint and the computational mesh in a high  
367 spatial resolution is characterized by a high number of mesh nodes per building. Thus, the flow depths  
368 of the mesh nodes have to be interpolated in some way to assign the flow depth to the building since  
369 this parameter is needed for computing the degree of loss and consequently the loss at single building  
370 scale. As the flow depth attribution method can significantly influence the outcomes of flood loss  
371 analyses, we recommend that the chosen method is explicitly described in future studies.

372 2) The attribution of the maximum flow depth of all nodes within the building footprint and a specified  
373 buffer distance to the building is robust. With this attribution method, the mesh set up (i.e., the method  
374 of representing the buildings in the computational mesh) does not significantly influence the loss  
375 estimation. In contrast, it becomes relevant when the flow depths are averaged over all nodes within  
376 the building. Herein, the nodes within the building footprint but representing the heights of the roof  
377 tops rather than the ground floor level result in flow depths of 0 m. Hence, these nodes should not be  
378 considered in averaging the flow depths. The mesh set up should thus be designed in line that it fits  
379 with the flow depth attribution method.

380 3) The exposure assessment is not highly sensitive to the building representation method. From this  
381 perspective, the benefits of using the more complex building representation methods in the flood  
382 inundation model are not clear. Results however showed that this low sensitivity to the mesh setup is  
383 valid for the maximum flow depth attribution method only. Hence, in low-density peri-urban  
384 environments, the way how to consider the buildings in the mesh is dependent on the flow depth  
385 attribution method and thus it plays a role for exposure and flood loss estimations. Hence, further  
386 analyses should be aimed at finding a threshold for building density that acts as a proxy for areas in  
387 which the building representation method is relevant or not.

388

### 389 **Software availability**

390 The flood loss model and the procedure for processing the IBER simulation outcomes are incorporated  
391 in a Python script. The code with the functions used in this study is available at GitHub  
392 <https://github.com/zischg/IBERfloodlossmodel>. The functions follow mainly the procedure described  
393 in the method section.

395 **Acknowledgements**

396 The authors thank the Swiss Federal Office for Statistics for providing the residential register, the  
 397 Swiss Federal Office for Topography for providing the building dataset, and the Canton of Bern,  
 398 Switzerland for providing the Lidar terrain model. María Bermúdez gratefully acknowledges financial  
 399 support from the Spanish Regional Government of Galicia (postdoctoral grant reference ED481B  
 400 2014/156-0). Andreas Paul Zischg gratefully acknowledges financial support from the Swiss National  
 401 Foundation (grant number IZK0Z2\_170478/1). The authors have no conflict of interest.

402

403 **References**

- 404 Abdullah AF, Vojinovic Z, Price RK, Aziz NAA (2012) Improved methodology for processing raw  
 405 LiDAR data to support urban flood modelling - accounting for elevated roads and bridges. *J*  
 406 *Hydroinformatics* 14:253–269 . doi: 10.2166/hydro.2011.009
- 407 Abily M, Bertrand N, Delestre O, et al (2016) Spatial Global Sensitivity Analysis of High Resolution  
 408 classified topographic data use in 2D urban flood modelling. *Environ Model Softw* 77:183–195 .  
 409 doi: 10.1016/J.ENVSOF.2015.12.002
- 410 Álvarez M, Puertas J, Peña E, Bermúdez M (2017) Two-Dimensional Dam-Break Flood Analysis in  
 411 Data-Scarce Regions: The Case Study of Chipembe Dam, Mozambique. *Water* 9:432 . doi:  
 412 10.3390/w9060432
- 413 Amadio M, Mysiak J, Carrera L, Koks E (2016) Improving flood damage assessment models in Italy.  
 414 *Nat Hazards* 82:2075–2088 . doi: 10.1007/s11069-016-2286-0
- 415 Apel H, Aronica GT, Kreibich H, Thielen AH (2009) Flood risk analyses—how detailed do we need  
 416 to be? *Nat Hazards* 49:79–98 . doi: 10.1007/s11069-008-9277-8
- 417 Apel H, Merz B, Thielen AH (2008) Quantification of uncertainties in flood risk assessments. *Int J*  
 418 *River Basin Manag* 6:149–162 . doi: 10.1080/15715124.2008.9635344
- 419 Apel H, Thielen AH, Merz B, Blöschl G (2006) A Probabilistic Modelling System for Assessing Flood  
 420 Risks. *Nat Hazards* 38:79–100 . doi: 10.1007/s11069-005-8603-7
- 421 Arrighi C, Brugioni M, Castelli F, et al (2013) Urban micro-scale flood risk estimation with  
 422 parsimonious hydraulic modelling and census data. *Nat Hazards Earth Syst Sci* 13:1375–1391 .  
 423 doi: 10.5194/nhess-13-1375-2013
- 424 Bellos V, Tsakiris G (2015) Comparing Various Methods of Building Representation for 2D Flood  
 425 Modelling In Built-Up Areas. *Water Resour Manag* 29:379–397 . doi: 10.1007/s11269-014-0702-  
 426 3
- 427 Bermúdez M, Neal JC, Bates PD, et al (2017) Quantifying local rainfall dynamics and uncertain  
 428 boundary conditions into a nested regional-local flood modeling system. *Water Resour Res*  
 429 53:2770–2785 . doi: 10.1002/2016WR019903
- 430 Bermúdez M, Ntegeka V, Wolfs V, Willems P (2018) Development and Comparison of Two Fast  
 431 Surrogate Models for Urban Pluvial Flood Simulations. *Water Resour Manag*. doi:  
 432 10.1007/s11269-018-1959-8
- 433 Bladé E, Cea L, Corestein G, et al (2014) Iber: herramienta de simulación numérica del flujo en ríos.  
 434 *Rev Int Métodos Numéricos para Cálculo y Diseño en Ing* 30:1–10 . doi:

435 10.1016/j.rimni.2012.07.004

436 Bodoque JM, Américo M, Díez-Herrero A, et al (2016) Improvement of resilience of urban areas by  
437 integrating social perception in flash-flood risk management. *J Hydrol* 541:665–676 . doi:  
438 10.1016/j.jhydrol.2016.02.005

439 Bonasia R, Areu-Rangel OS, Tolentino D, et al (2017) Flooding hazard assessment at Tulancingo  
440 (Hidalgo, Mexico). *J Flood Risk Manag.* doi: 10.1111/jfr3.12312

441 Cammerer H, Thielen AH, Lammel J (2013) Adaptability and transferability of flood loss functions  
442 in residential areas. *Nat Hazards Earth Syst Sci* 13:3063–3081 . doi: 10.5194/nhess-13-3063-2013

443 Cea L, Bermudez M, Puertas J, et al (2016) IberWQ: new simulation tool for 2D water quality  
444 modelling in rivers and shallow estuaries. *J Hydroinformatics* 18:816–830 . doi:  
445 10.2166/hydro.2016.235

446 Cea L, Vázquez-Cendón ME (2009) Unstructured finite volume discretization of two-dimensional  
447 depth-averaged shallow water equations with porosity. *Int J Numer Methods Fluids* 63:n/a-n/a .  
448 doi: 10.1002/fld.2107

449 Chen AS, Evans B, Djordjević S, et al (2012a) A coarse-grid approach to representing building blockage  
450 effects in 2D urban flood modelling. *J Hydrol* 1–16 . doi: 10.1016/j.jhydrol.2012.01.007

451 Chen AS, Evans B, Djordjević S, Savić DA (2012b) Multi-layered coarse grid modelling in 2D urban  
452 flood simulations. *J Hydrol* 470:1–11 . doi: 10.1016/j.jhydrol.2012.06.022

453 Davis SA, Skaggs LL (1992) Catalog of Residential Depth-Damage Functions used by the Army Corps  
454 of Engineers in Flood Damage Estimation

455 de Almeida GAM, Bates P, Ozdemir H (2016) Modelling urban floods at sub-metre resolution:  
456 challenges or opportunities for flood risk management? *J Flood Risk Manag.* doi:  
457 10.1111/jfr3.12276

458 de Moel H, Aerts JCJH (2011) Effect of uncertainty in land use, damage models and inundation depth  
459 on flood damage estimates. *Nat Hazards* 58:407–425 . doi: 10.1007/s11069-010-9675-6

460 Dutta D, Herath S, Musiak K (2003) A mathematical model for flood loss estimation. *J Hydrol*  
461 277:24–49 . doi: 10.1016/S0022-1694(03)00084-2

462 Environment Agency (2014) The updated Flood Map for Surface Water (uFMfSW) Property Points  
463 dataset.

464 Ernst J, Dewals BJ, Detrembleur S, et al (2010) Micro-scale flood risk analysis based on detailed 2D  
465 hydraulic modelling and high resolution geographic data. *Nat Hazards* 55:181–209 . doi:  
466 10.1007/s11069-010-9520-y

467 Fewtrell TJ, Bates PD, Horritt M, Hunter NM (2008) Evaluating the effect of scale in flood inundation  
468 modelling in urban environments. *Hydrol Process* 22:5107–5118 . doi: 10.1002/hyp.7148

469 Fewtrell TJ, Duncan A, Sampson CC, et al (2011) Benchmarking urban flood models of varying  
470 complexity and scale using high resolution terrestrial LiDAR data. *Phys Chem Earth* 36:281–291  
471 . doi: 10.1016/j.pce.2010.12.011

472 Freni G, La Loggia G, Notaro V (2010) Uncertainty in urban flood damage assessment due to urban  
473 drainage modelling and depth - damage curve estimation. *Water Sci Technol* 61:2979–2993 . doi:  
474 10.2166/wst.2010.177

475 Fuchs S, Birkmann J, Glade T (2012) Vulnerability assessment in natural hazard and risk analysis:  
476 current approaches and future challenges. *Nat Hazards* 64:1969–1975 . doi: 10.1007/s11069-012-  
477 0352-9

478 Fuchs S, Keiler M, Zischg A (2015) A spatiotemporal multi-hazard exposure assessment based on  
479 property data. *Nat Hazards Earth Syst Sci* 15:2127–2142 . doi: 10.5194/nhess-15-2127-2015

480 Fuchs S, Röthlisberger V, Thaler T, et al (2017) Natural Hazard Management from a Coevolutionary

481 Perspective: Exposure and Policy Response in the European Alps. *Ann Am Assoc Geogr*  
482 107:382–392 . doi: 10.1080/24694452.2016.1235494

483 Garrote J, Alvarenga FM, Díez-Herrero A (2016) Quantification of flash flood economic risk using  
484 ultra-detailed stage–damage functions and 2-D hydraulic models. *J Hydrol* 541:611–625 . doi:  
485 10.1016/j.jhydrol.2016.02.006

486 González-Aguirre JC, Vázquez-Cendón ME, Alavez-Ramírez J (2016) Simulación numérica de  
487 inundaciones en Villahermosa México usando el código IBER. *Ing del agua* 20:201 . doi:  
488 10.4995/ia.2016.5231

489 Green CH (2003) *The handbook of water economics : principles and practice*. Wiley

490 Guinot V (2012) Multiple porosity shallow water models for macroscopic modelling of urban floods.  
491 *Adv Water Resour* 37:40–72 . doi: 10.1016/j.advwatres.2011.11.002

492 Horritt M., Bates PD (2002) Evaluation of 1D and 2D numerical models for predicting river flood  
493 inundation. *J Hydrol* 268:87–99 . doi: 10.1016/S0022-1694(02)00121-X

494 Hydrotec (2001) *Hochwasser-Aktionsplan Angerbach (Flood action plan for the river Angerbach).*  
495 *Teil I: Berichte und Anlagen. Studie im Auftrag des Stua Dusseldorf. Aachen, Germany*

496 Jonkman SN, Bočkarjova M, Kok M, Bernardini P (2008) Integrated hydrodynamic and economic  
497 modelling of flood damage in the Netherlands. *Ecol Econ* 66:77–90 . doi:  
498 10.1016/j.ecolecon.2007.12.022

499 Kreibich H, Piroth K, Seifert I, et al (2009) Is flow velocity a significant parameter in flood damage  
500 modelling? *Nat Hazards Earth Syst Sci* 9:1679–1692

501 Kumar M, Bhatt G, Duffy CJ (2009) An efficient domain decomposition framework for accurate  
502 representation of geodata in distributed hydrologic models. *Int J Geogr Inf Sci* 23:1569–1596 .  
503 doi: 10.1080/13658810802344143

504 McGrath H, Stefanakis E, Nastev M (2015) Sensitivity analysis of flood damage estimates: A case  
505 study in Fredericton, New Brunswick. *Int J Disaster Risk Reduct* 14:379–387 . doi:  
506 10.1016/J.IJDRR.2015.09.003

507 Merz B, Kreibich H, Schwarze R, Thielen A (2010) Assessment of economic flood damage. *Nat*  
508 *Hazards Earth Syst Sci* 10:1697–1724 . doi: 10.5194/nhess-10-1697-2010

509 Merz B, Thielen AH (2009) Flood risk curves and uncertainty bounds. *Nat Hazards* 51:437–458 . doi:  
510 10.1007/s11069-009-9452-6

511 Notaro V, De Marchis M, Fontanazza CM, et al (2014) The Effect of Damage Functions on Urban  
512 Flood Damage Appraisal. *Procedia Eng* 70:1251–1260 . doi: 10.1016/J.PROENG.2014.02.138

513 Ozdemir H, Sampson CC, de Almeida GAM, Bates PD (2013) Evaluating scale and roughness effects  
514 in urban flood modelling using terrestrial LIDAR data. *Hydrol Earth Syst Sci* 17:4015–4030 .  
515 doi: 10.5194/hess-17-4015-2013

516 Papathoma-Köhle M, Gems B, Sturm M, Fuchs S (2017) Matrices, curves and indicators: A review of  
517 approaches to assess physical vulnerability to debris flows. *Earth-Science Rev* 171:272–288 . doi:  
518 10.1016/J.EARSCIREV.2017.06.007

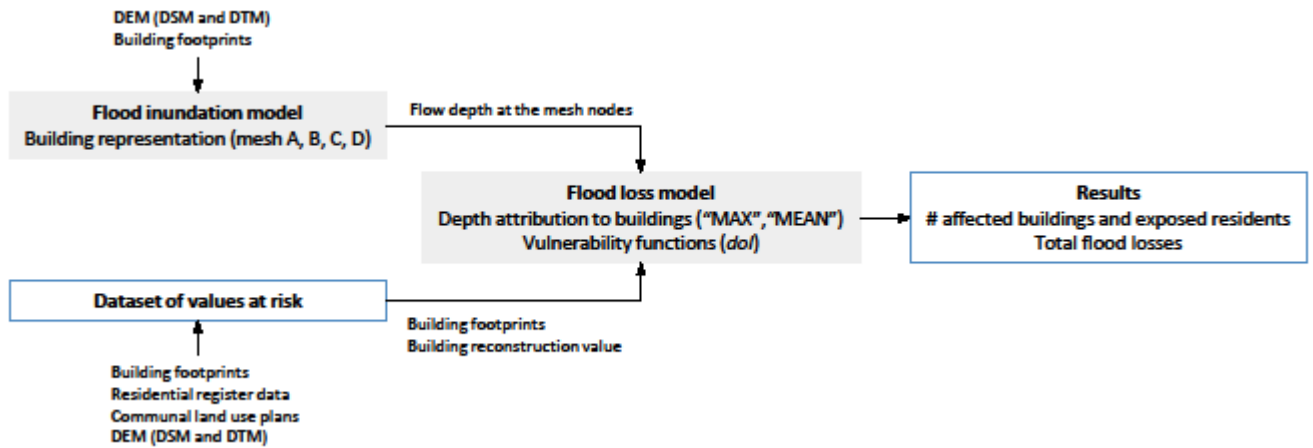
519 Papathoma-Köhle M, Zischg A, Fuchs S, et al (2015) Loss estimation for landslides in mountain areas  
520 – An integrated toolbox for vulnerability assessment and damage documentation. *Environ Model*  
521 *Softw* 63:156–169 . doi: 10.1016/J.ENVSOFT.2014.10.003

522 Qi H, Altinakar MS (2011) Simulation-based decision support system for flood damage assessment  
523 under uncertainty using remote sensing and census block information. *Nat Hazards* 59:1125–1143  
524 . doi: 10.1007/s11069-011-9822-8

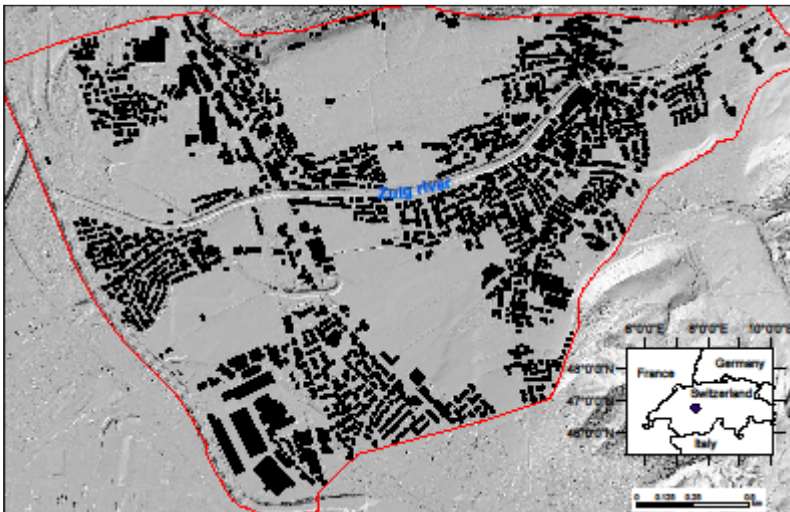
525 Röthlisberger V, Zischg AP, Keiler M (2017) Identifying spatial clusters of flood exposure to support  
526 decision making in risk management. *Sci Total Environ* 598:593–603 . doi:

527 10.1016/j.scitotenv.2017.03.216  
528 Sampson CC, Fewtrell TJ, Duncan A, et al (2012) Use of terrestrial laser scanning data to drive  
529 decimetric resolution urban inundation models. *Adv Water Resour* 41:1–17 . doi:  
530 10.1016/j.advwatres.2012.02.010  
531 Sampson CC, Fewtrell TJ, O’Loughlin F, et al (2014) The impact of uncertain precipitation data on  
532 insurance loss estimates using a flood catastrophe model. *Hydrol Earth Syst Sci* 18:2305–2324 .  
533 doi: 10.5194/hess-18-2305-2014  
534 Schubert JE, Sanders BF (2012) Building treatments for urban flood inundation models and  
535 implications for predictive skill and modeling efficiency. *Adv Water Resour* 41:49–64 . doi:  
536 10.1016/j.advwatres.2012.02.012  
537 Staffler H, Pollinger R, Zischg A, Mani P (2008) Spatial variability and potential impacts of climate  
538 change on flood and debris flow hazard zone mapping and implications for risk management. *Nat*  
539 *Hazards Earth Syst Sci* 8:539–558 . doi: 10.5194/nhess-8-539-2008  
540 Totschnig R, Sedlacek W, Fuchs S (2011) A quantitative vulnerability function for fluvial sediment  
541 transport. *Nat Hazards* 58:681–703 . doi: 10.1007/s11069-010-9623-5  
542 Zischg A, Schober S, Sereinig N, et al (2013) Monitoring the temporal development of natural hazard  
543 risks as a basis indicator for climate change adaptation. *Nat Hazards* 67:1045–1058 . doi:  
544 10.1007/s11069-011-9927-0  
545 Zischg AP, Mosimann M, Bernet DB, Röthlisberger V (2018) Validation of 2D flood models with  
546 insurance claims. *J Hydrol* 557:350–361 . doi: 10.1016/J.JHYDROL.2017.12.042  
547  
548

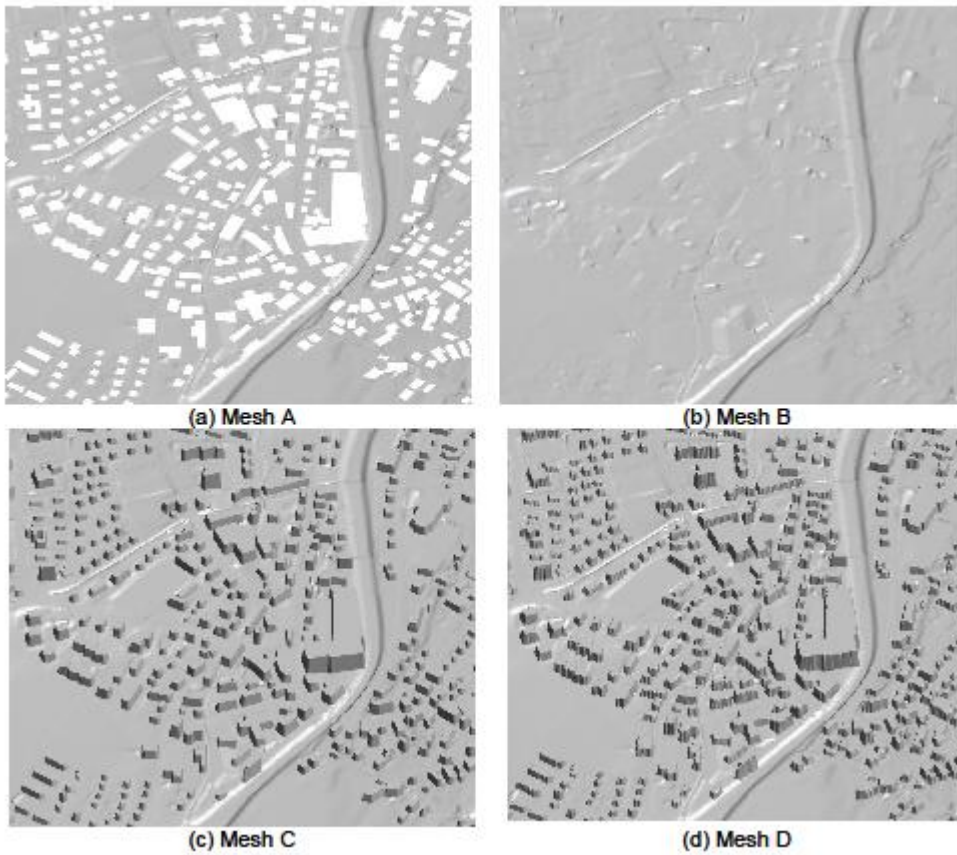
549 **FIGURES**



550  
551 **Fig. 1** Flow diagram of the methodology: flood inundation model, flood loss model and dataset of  
552 values at risk.

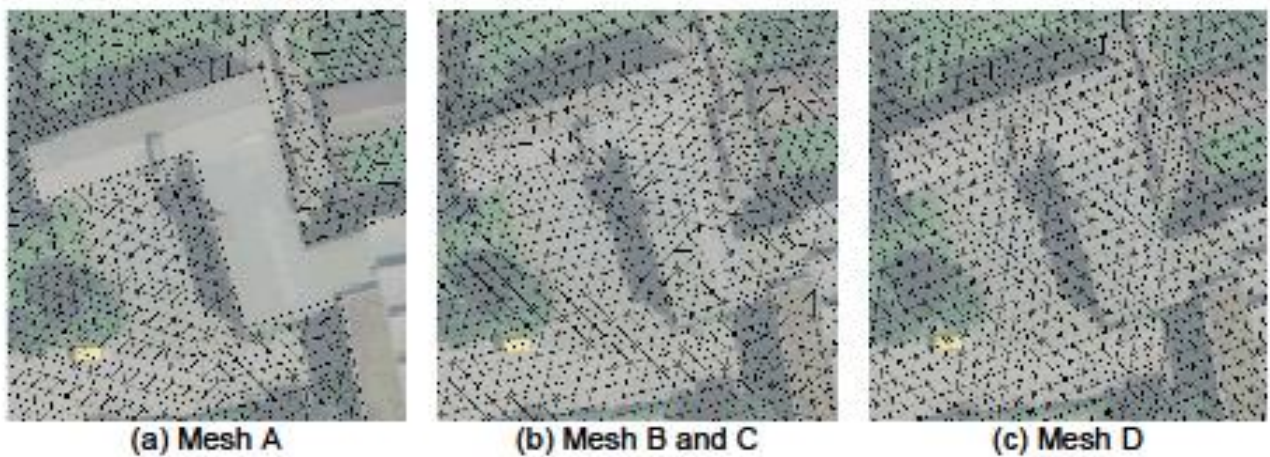


553  
554 **Fig. 2** Extent of the study area. The Zulg river flows from NE to E through the village of Steffisburg.  
555



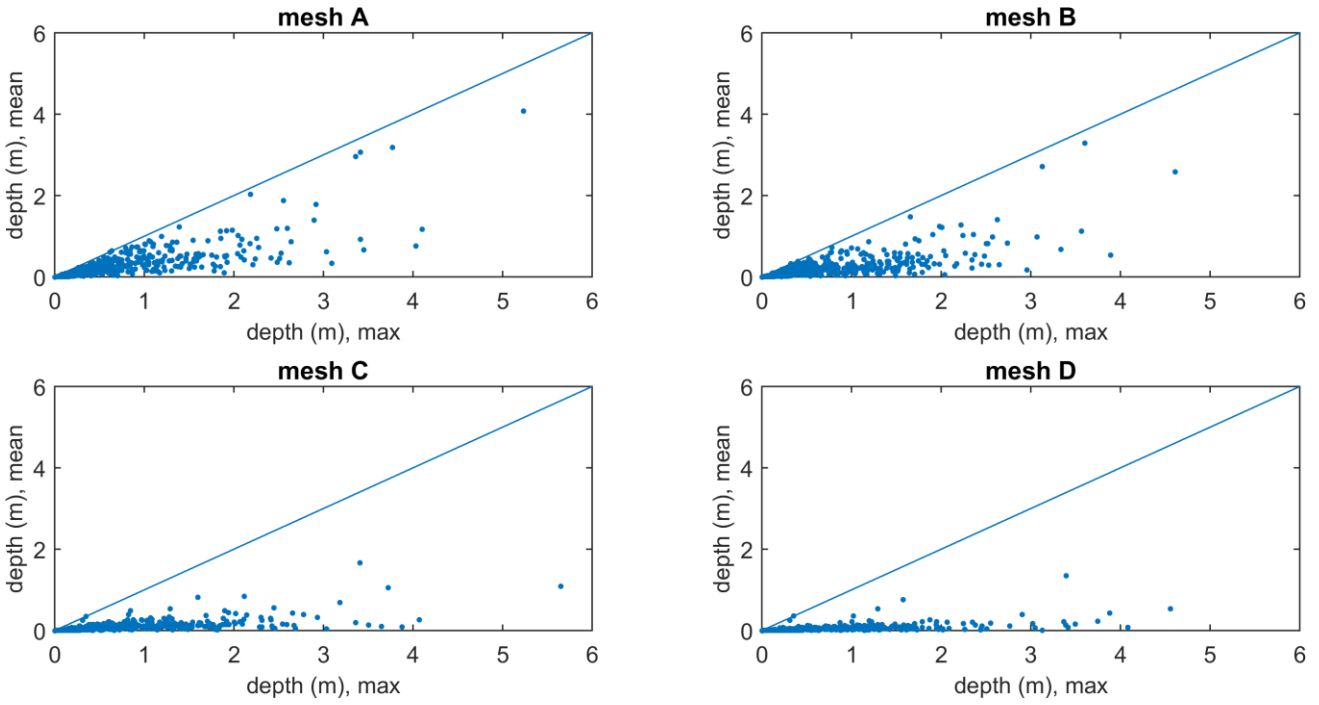
556

557 **Fig. 3** Mesh geometries with different representation of the buildings (3D view). In (a), buildings are  
 558 represented as holes, while in (b), (c) and (d) the area covered by the buildings is part of the mesh. The  
 559 z-coordinates of the nodes within the building footprints equal the values of the DTM in (b) and the  
 560 values of the DSM in (c) and (d).



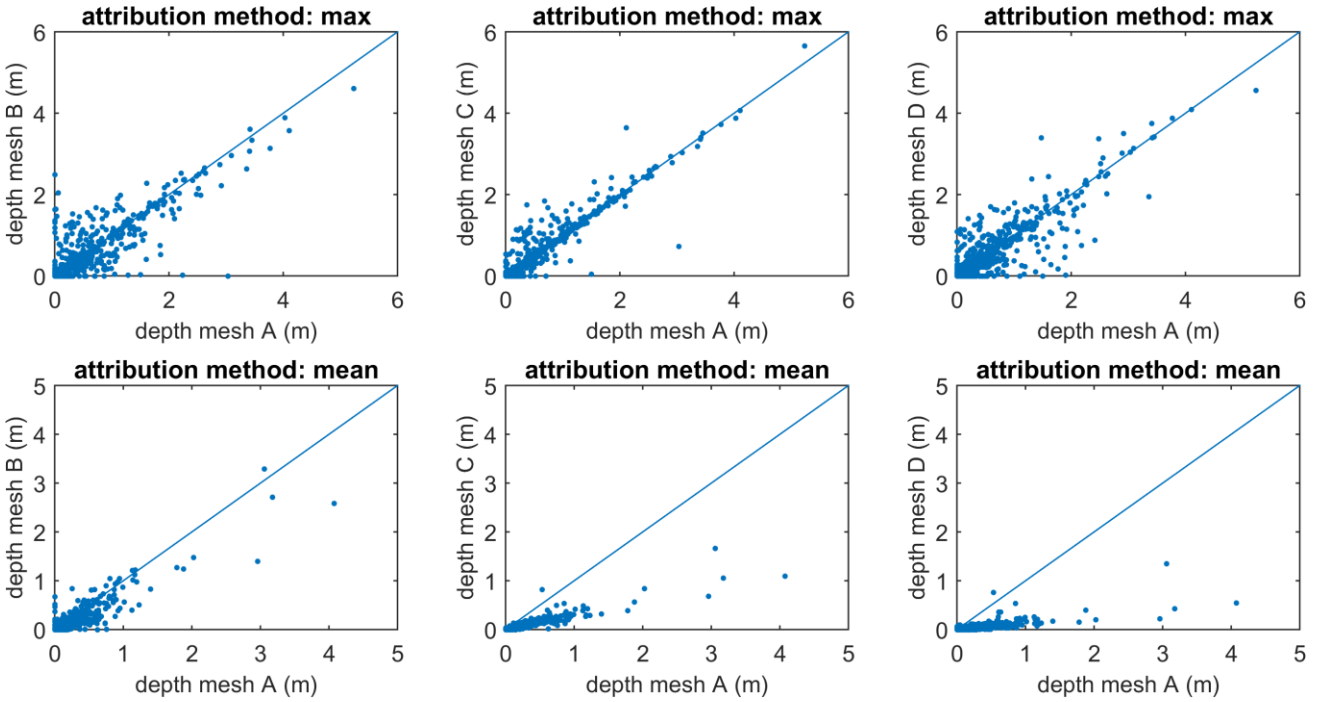
561

562 **Fig. 4** Detail of the mesh around a building, overlaid on an aerial image. Mesh B and C are identical  
 563 in this plan view, although elevations assigned to the nodes within the building footprint differ.  
 564 Building footprints serve as constraints for mesh generation in mesh A, B and C.



565

566 **Fig. 5** Scatter plot of depth values assigned to each building with the different hazard attribution  
 567 methods.



568

569 **Fig. 6** Scatter plot of depth values assigned to each building with the different mesh configurations.  
 570